

## Article

# Multi-Isotopic Compositions of Ores from the Shizishan Cu–Au–Mo Orefield in the Tongling Region, Eastern China: Implications for Ore Genesis

Jinwei Li <sup>1</sup> , Lichuan Pan <sup>2,\*</sup>, Yitong Guo <sup>1</sup> and Shunfu Lu <sup>2</sup><sup>1</sup> Research Center of Ancient Ceramic, Jingdezhen Ceramic University, Jingdezhen 333403, China<sup>2</sup> State Key Laboratory of Ore Deposit Geochemistry, Institute of Geochemistry, Chinese Academy of Sciences, Guiyang 550081, China

\* Correspondence: panlichuan@mail.gyig.ac.cn

**Abstract:** The Middle–Lower Yangtze Metallogenic Belt (MLYMB) hosts abundant porphyry–skarn–stratabound-type Cu–Au–Mo deposits. Despite extensive research, the origin of the stratabound-type deposits, which developed at the unconformity interface between the Devonian and Carboniferous strata in the MLYMB, remains controversial. The primary debate centers on whether these deposits are the result of Carboniferous sedimentary exhalative mineralization or Mesozoic magmatic–hydrothermal mineralization. In this paper, we examine three representative deposits in the Shizishan orefield: the Chaoshan skarn-type Au deposit, the Hucun porphyry–skarn-type Cu–Mo deposit, and the Dongguashan Cu–(Au) deposit, which has a disputed genesis of its stratiform orebodies. Economically important ore minerals, such as chalcopyrite, molybdenite, and pyrrhotite, and their associated quartz and calcite, were focused on, rather than the extensively studied pyrite in the Tongling region. The ore genesis and sources of mineralized elements in the Shizishan orefield were investigated using H, O, C, S, Pb, and Cu isotopes. The H–O isotopic compositions of hydrothermal quartz from the Chaoshan, Dongguashan, and Hucun deposits indicate that the ore-forming fluids were mainly magmatic water with some meteoric water input. The C–O isotopic compositions of calcite show a large difference from the local sedimentary carbonates. The S isotopic compositions of sulfides reveal a magmatic sulfur signature. The Pb isotopic compositions in the three deposits are similar to those of the Shizishan intrusions, suggesting a magmatic source for Pb. The Cu isotopic compositions of chalcopyrite and pyrrhotite demonstrate that Cu, the primary ore-forming element, was mainly derived from magmatic–hydrothermal fluids. The stratiform orebodies display H–O–C–S–Pb–Cu isotopes consistent with the porphyry orebodies in the Dongguashan deposit, as well as in the Chaoshan and Hucun deposits, indicating a common ore genesis. From these, we conclude that the porphyry–skarn–stratabound-type Cu–Au–Mo deposits in the Shizishan orefield can be classified as a unified Mesozoic magmatic–hydrothermal metallogenic system. The stratabound-type copper sulfide deposits and the porphyry–skarn-type copper deposits in the MLYMB have a strong similarity in the source and genesis of their ore-forming elements.

**Keywords:** H–O–C–S–Pb–Cu isotopes; magmatic–hydrothermal mineralization; ore genesis; Shizishan Cu–Au–Mo orefield; Middle–Lower Yangtze Metallogenic Belt



**Citation:** Li, J.; Pan, L.; Guo, Y.; Lu, S. Multi-Isotopic Compositions of Ores from the Shizishan Cu–Au–Mo Orefield in the Tongling Region, Eastern China: Implications for Ore Genesis. *Minerals* **2023**, *13*, 985. <https://doi.org/10.3390/min13070985>

Academic Editor:  
Panagiotis Voudouris

Received: 3 July 2023  
Revised: 14 July 2023  
Accepted: 19 July 2023  
Published: 24 July 2023



**Copyright:** © 2023 by the authors. Licensee MDPI, Basel, Switzerland. This article is an open access article distributed under the terms and conditions of the Creative Commons Attribution (CC BY) license (<https://creativecommons.org/licenses/by/4.0/>).

## 1. Introduction

The Middle–Lower Yangtze Metallogenic Belt (MLYMB), a significant metallic province in China (Figure 1), is renowned for its abundance of porphyry–skarn–stratabound-type Cu–Au–Mo deposits [1–3] and porphyrite-type Fe deposits [4–6]. Notably, stratabound copper sulfide deposits, such as the Xinqiao, Dongguashan, and Wushan deposits, exhibit layered or quasi-layered mineralization occurring at the unconformable interface between Carboniferous carbonate strata and Devonian siliceous strata. The origin of these deposits has been a subject of considerable debate with two main viewpoints. One proposes that

the stratabound copper sulfide deposits primarily represent Carboniferous exhalative massive sulfide layers that have been modified and overprinted by Mesozoic magmas and hydrothermal fluids [7–11], while the other suggests that a substantial deposition of pyrite occurred during the Carboniferous, while Cu, Au, and Mo were supplied by Mesozoic magmatic–hydrothermal processes [1,2,12–20].

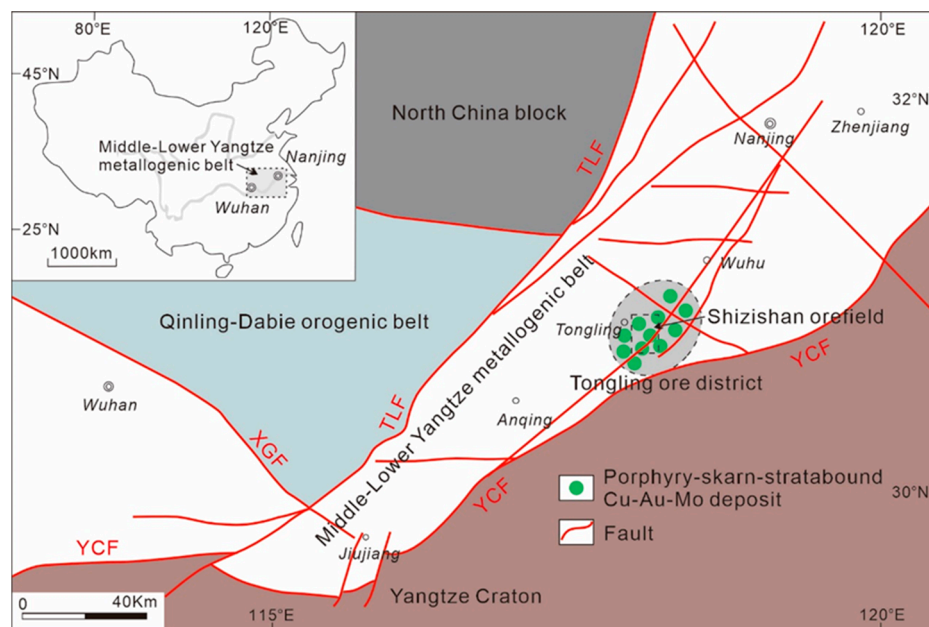


**Figure 1.** Simplified structural map showing the locations of the Middle–Lower Yangtze metallogenic belt, the Tongling ore district, and the Shizishan orefield (Modified from [2]).

From the mineral assemblages, it can be observed that massive sulfides, tuffaceous rocks, hydrothermal breccias, laminated pyrite, and argillaceous limestone at the bottom of the Carboniferous strata are components of submarine sediments [21], confirming the presence of exhalative sedimentation. Some scholars have compared the sulfur isotope ratios of pyrite in the stratabound-type deposits and regional sulfates, which also support the theory that their origin is exhalative sedimentation [22,23]. However, other researchers have obtained sulfur isotope values of sulfides in the stratabound-type deposits that indicate deep magmatic sources [13,17,20,24]. Based on the Rb–Sr and Re–Os isotope dating of pyrite in the stratabound-type deposits, two sets of ages have been identified: one for the Carboniferous period [10,22,25] and the other for the Mesozoic period [26–28], suggesting at least two episodes of hydrothermal events for pyrite precipitation. Nevertheless, the Re–Os isotope ages of molybdenite consistently show a Mesozoic mineralization age [29–31], and U–Pb dating results of hydrothermal apatite and hematite also support the theory of Mesozoic magmatic–hydrothermal mineralization [19]. Evidently, previous studies on pyrite in the stratabound-type deposits have often yielded contradictory conclusions. This may be attributed to the generation of pyrite during multiple geological events and its potential modification by later magmatic–hydrothermal fluids. Hence, the main ore minerals related to Cu, Au, and Mo, such as chalcopyrite, molybdenite, and pyrrhotite, may offer more reliable insights into the mineralization processes.

The Tongling region is an important district of Cu–Au–Mo mineralization in the MLYRMB. Situated in the western part of the Tongling region, the Shizishan orefield hosts several porphyry–skarn–stratabound-type Cu–Au–Mo deposits (Figure 1). Our research focuses on three representative deposits within the Shizishan orefield: the Chaoshan deposit, characterized as a skarn-type Au deposit [32,33]; the Hucun deposit, recognized as a porphyry–skarn-type Cu–Mo deposit [34,35]; and the Dongguashan deposit, which is a Cu–(Au) deposit with a disputed genesis of its stratiform orebodies [24,36]. Stable isotopic compositions have proven to be effective in identifying the sources of mineralized elements

and elucidating ore genesis. In this study, instead of examining extensively studied pyrite in the Tongling region, we concentrate on economically important ore minerals, including chalcopyrite, molybdenite, and pyrrhotite, as well as their associated quartz and calcite. We have utilized sulfur, carbon, oxygen, hydrogen, lead, and copper isotopic compositions to investigate the ore genesis and sources of mineralized elements in the Shizishan orefield. The newly obtained data significantly contribute to enhancing our understanding of the genesis of stratabound copper sulfide deposits within the MLYMB.

## 2. Geology Background

### 2.1. Regional Geology

As shown in Figure 1, the MLYMB is positioned on the northern margin of the Yangtze Block and to the east of the Qinling–Dabie orogenic belt and the North China Block. The geodynamic evolution of the MLYMB can be attributed to several key events, including the formation of a Precambrian metamorphic basement, the deposition of Paleozoic–Mesozoic sedimentary rocks, and the Middle Triassic collision between the North China Block and the Yangtze Block [1]. During the Late Jurassic to Early Cretaceous, post-collisional extension caused lithospheric delamination and resulted in extensive magmatism [37,38]. Concurrently, the Paleo–Pacific plate subducted beneath eastern China [39,40]. These large-scale Mesozoic magmatic–hydrothermal activities led to the formation of numerous plutons with Cu, Au, Fe, and Mo mineralization.

The Shizishan orefield is located to the west of the Tongling region (Figure 1). In this area, the main exposed strata consist of Triassic carbonates. The Mesozoic intrusions, covering an outcrop area of approximately 3.0 km<sup>2</sup>, primarily consist of pyroxene diorite, quartz diorite, and granodiorite [13]. The spatial distribution of several Au and Cu–(Mo) deposits in close proximity to these intrusions indicates a significant relationship between mineralization and magma intrusive activities (Figure 2).

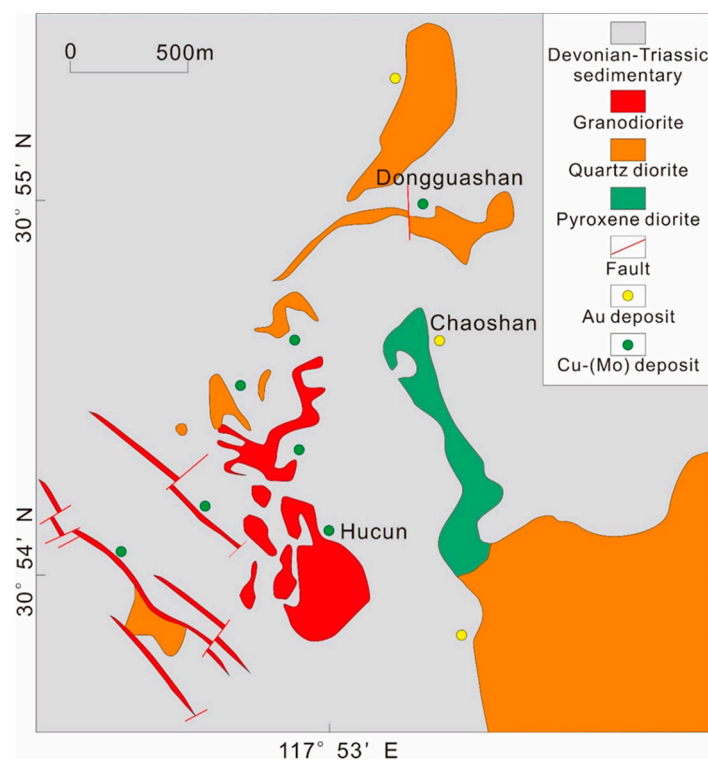


**Figure 2.** Simplified geological map of the Shizishan orefield in the Tongling region (modified from [32]).

### 2.2. Chaoshan Au Deposit

Situated in the central part of the Shizishan orefield, the Chaoshan Au deposit is classified as a skarn-type deposit [33,41]. The Au-mineralized intrusion in Chaoshan predominantly comprises pyroxene diorite, characterized by approximately 70% plagioclase, 10% pyroxene, 15% hornblende, and 5% biotite [32]. Skarns, exhibiting a typical prograde mineralogy of garnet, diopside, and scapolite, are found in or near the contact zone between the pyroxene diorite intrusions and the adjacent limestone sediments (Figure 3A). The absence of magnetite and hematite, coupled with the abundance of pyrrhotite, indicates the reducing type of the skarns [42].

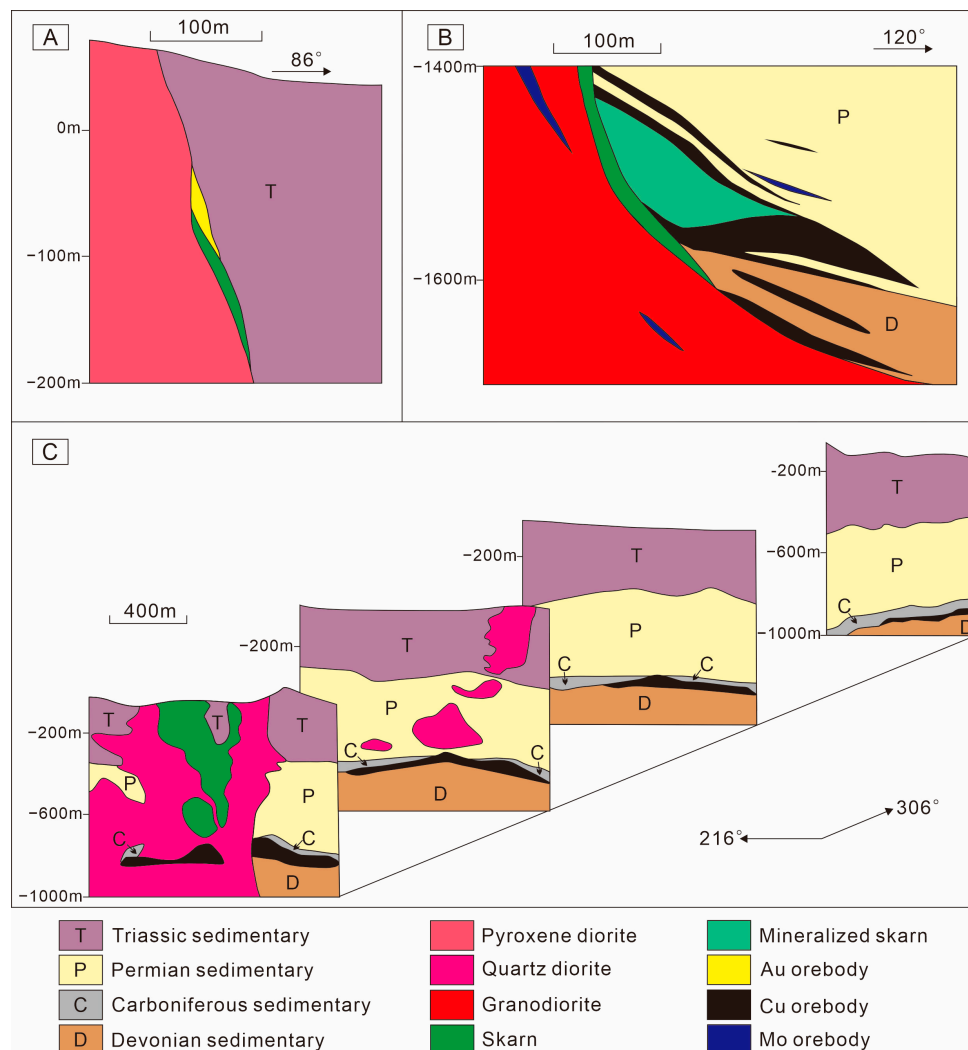


**Figure 3.** Geological cross sections of the Chaoshan (A), Hucun (B), and Dongguashan (C) deposits in the Shizishan orefield (modified from [14]).

The deposit includes ten orebodies that predominantly exhibit a lenticular and podiform shape, located along the intrusion–sedimentary contact zone. Gold mineralization mainly occurred as native Au inclusions within pyrrhotite, pyrite, arsenopyrite, chalcopyrite, and sphalerite, with pyrrhotite being the prime carrier mineral (Figure 4A–C). The gold grades range from 6 to 38 g/t, with an average of 18.4 g/t [14]. The Re–Os isochron age of the Au-bearing pyrrhotite is determined to be  $141.7 \pm 9.9$  Ma [41], which aligns with the zircon U–Pb age of the associated pyroxene diorite ( $139.6 \pm 2.1$ ) [14]. These ages support a close genetic relationship between the pyroxene diorite and the Au mineralization.

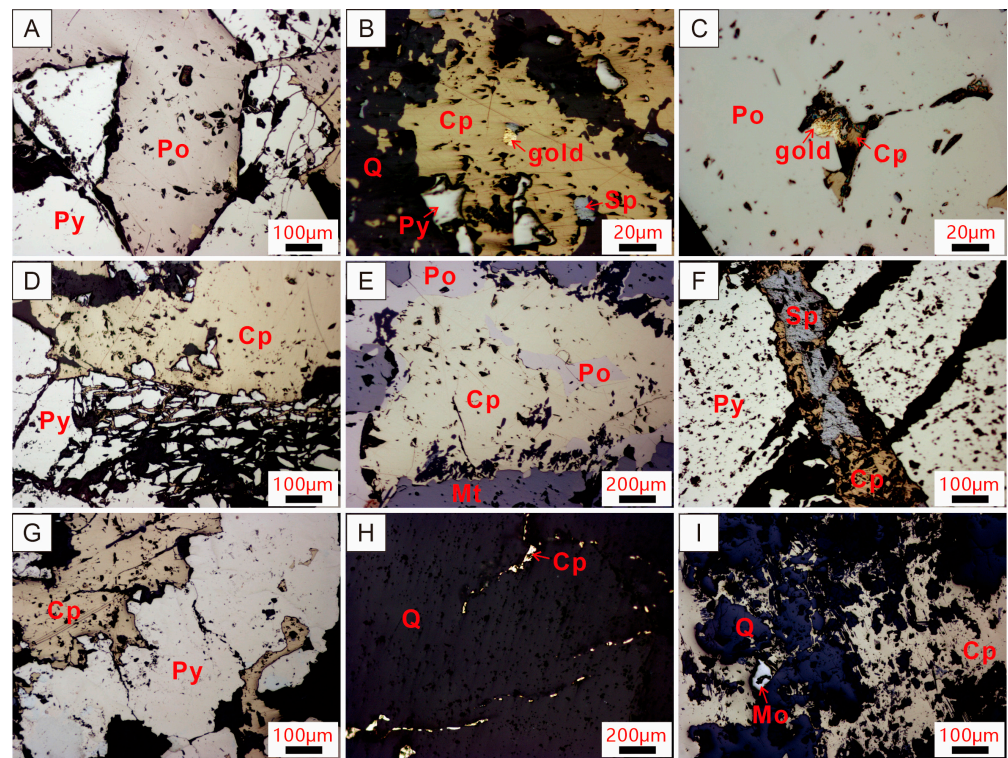


**Figure 4.** Photomicrographs of the ore minerals in the Chaoshan deposit (A–C), the Dongguashan deposit (D–F), and the Hucun deposit (G–I). Abbreviations: Py = pyrite; Po = pyrrhotite; Cp = chalcopyrite; Sp = sphalerite; Mt = magnetite; Mo = molybdenite; Q = quartz. (A) Pyrrhotite replaced pyrite. (B) Native Au inclusion in chalcopyrite. (C) Native Au and chalcopyrite inclusions in pyrrhotite. (D) Pyrite was dissolved and replaced by chalcopyrite–quartz vein. (E) Magnetite was replaced by chalcopyrite–pyrrhotite aggregate. (F) Chalcopyrite–sphalerite vein across pyrite. (G) Chalcopyrite replaced pyrite. (H) Chalcopyrite distributed along cracks in quartz crystal. (I) Chalcopyrite coexisted with molybdenite in quartz vein.

### 2.3. Hucun Cu–Mo Deposit

The Hucun Cu–Mo deposit is situated in the southern part of the Shizishan orefield. The Hucun granodiorite ( $140.9 \pm 1.2$  Ma) [43], which intruded Carboniferous–Triassic sedimentary strata (Figure 3B), is closely associated with the Cu–Mo mineralization. The granodiorite comprises approximately 40% plagioclase, 25% quartz, 15% K-feldspar, 15% hornblende, and 5% biotite [32].

The deposit is divided into two categories: shallow Cu orebodies and deep Cu–Mo orebodies. The shallow orebodies, which are located in the contact zone between the granodiorite and carbonate wall-rocks, exhibit characteristics indicative of skarn-type mineralization [14]. The deep orebodies are distributed within the granodiorite and the granodiorite–carbonate contact zone, occurring at a depth of more than 1000 m below the current surface (Figure 3B), characterized as a mixture genesis of porphyry-type and skarn-type. The Cu grade ranges from 0.4 to 0.8%, while the Mo grade ranges from 0.07 to 0.12% [34]. The main ore minerals include chalcopyrite, pyrite, molybdenite, and other sulfides (Figure 4G–I). Molybdenite in the mineralized intrusion exhibits a Re–Os isochron age of  $139.5 \pm 1.1$  Ma [44], representing the ore-forming age.

### 2.4. Dongguashan Cu–(Au) Deposit

The Dongguashan Cu–(Au) deposit is located to the north of the Shizishan orefield. The exposed strata in the mining area consist of Triassic carbonates. The ore-bearing sequence comprises Upper Devonian sandstone and shale, Middle–Upper Carboniferous limestone (Figure 3C), and Lower Permian limestone, quartzite, and skarn. The Dong-

guashan intrusion consists of medium- to coarse-grained quartz diorite, with approximately 60% plagioclase, 15% quartz, 15% hornblende, 5% biotite, and 5% K-feldspar [32]. The zircon U–Pb age of the Dongguashan intrusion ranges from 136 to 142 Ma [11,14].

Based on mineral exploration findings, the deposit includes four types of orebodies: stratiform type, porphyry type, skarn type, and vein-like type [45]. Among these, the stratiform type is considered the most significant [24]. The stratiform orebodies occur in the Middle–Upper Carboniferous limestone and the unconformity interface between the Upper Devonian quartz sandstone and the Middle–Upper Carboniferous limestone. The thickness of the orebodies near the intrusion is substantial, gradually thinning as they move away from the intrusion until they are eventually pinched out (Figure 3C). The stratiform orebodies contain pyrrhotite, pyrite, and chalcopyrite (Figure 4D), and very little native gold [13]. There is no conclusive evidence to determine whether the stratiform orebodies were formed during the Carboniferous or the Mesozoic. The porphyry orebodies occur in the intrusion, primarily comprising pyrite, chalcopyrite, and pyrrhotite as the ore minerals (Figure 4F). Skarn-type ore bodies are mainly distributed in the contact zone between the intrusion and carbonate, and their primary ore minerals include chalcopyrite, magnetite, pyrrhotite, and pyrite (Figure 4E) [24]. Besides the stratiform orebodies, the formation ages of other types of ore bodies are consistent with the age of the Dongguashan intrusion, occurring approximately around 140 Ma [13,36].

### 3. Sampling and Analytical Methods

#### 3.1. Samples

Samples of the Chaoshan deposit were collected from the ZK-5 drill core and underground adits of –120 m below sea level. For the Dongguashan deposit, samples were obtained from the ZK-905 drill core and underground adits of –700 m, –750 m, and –850 m below sea level. Regarding the Hucun deposit, samples were extracted from the ZK-941 and ZK-945 drill cores. The collected hand specimens were crushed to a particle size of 300  $\mu\text{m}$  and then carefully handpicked under a binocular microscope. Chalcopyrite, pyrrhotite, molybdenite, quartz, and calcite were selected and ground to 60  $\mu\text{m}$  size for isotopic analysis. X-ray diffraction analysis was performed on the samples to ensure >99% purity.

#### 3.2. Analytical Methods

Hydrogen and oxygen isotope analyses of quartz were performed with a Thermo Scientific Finnigan MAT-253 mass spectrometer at the Analytical Laboratory of Beijing Research Institute of Uranium Geology, Beijing, China. Oxygen was liberated from quartz through a reaction with  $\text{BrF}_5$  and subsequently reacted with graphite rods to produce  $\text{CO}_2$  [46]. The water within the fluid inclusions in the quartz samples was released by heating the samples to temperatures above 500  $^\circ\text{C}$  in an induction furnace. The fluid inclusions were then reacted with zinc powder to generate  $\text{H}_2$  [47]. The H–O isotopic data were reported in per mil units relative to V-SMOW. The precision values were  $\pm 0.2\text{‰}$  ( $2\sigma$ ) for  $\delta^{18}\text{O}$  and  $\pm 2\text{‰}$  ( $2\sigma$ ) for  $\delta\text{D}$ .

Carbon and oxygen isotope analyses of calcite, as well as sulfur isotope analyses of sulfides, were conducted using a Finnigan MAT-253 mass spectrometer at the State Key Laboratory of Ore Deposit Geochemistry, Chinese Academy of Sciences. The calcite samples underwent a reaction with pure phosphoric acid to generate  $\text{CO}_2$  [48]. The results were reported in per mil units relative to the V-PDB standard, with a precision of  $\pm 0.2\text{‰}$  ( $2\sigma$ ) for  $\delta^{18}\text{O}$  and  $\pm 0.1\text{‰}$  ( $2\sigma$ ) for  $\delta^{13}\text{C}$ . To obtain the sulfur isotopic ratios, the sulfides were reacted with  $\text{Cu}_2\text{O}$  powder to produce  $\text{SO}_2$  [49]. The sulfur isotopic ratios were given in per mil units relative to the V-CDT standard with a precision of  $\pm 0.2\text{‰}$  ( $2\sigma$ ).

Lead isotope analyses of sulfides were analyzed with a MicroMass ISOPROBE-T Thermal Ionization Mass Spectrometer (TIMS) at the State Key Laboratory of Geological Process and Mineral Resources, China University of Geosciences, Beijing, China. The Pb was separated and purified using a cation-exchange technique, following the procedure

of [50], with diluted HBr used as the eluant. The analytical precision was better than  $\pm 0.005\%$  for  $^{208}\text{Pb}/^{206}\text{Pb}$  ( $2\sigma$ ).

Copper isotope compositions of chalcopyrite and pyrrhotite were analyzed with a Thermo Scientific Neptune Plus multiple collector inductively coupled plasma mass spectrometer (MC-ICP-MS) at the State Key Laboratory of Geological Process and Mineral Resources, China University of Geosciences, Beijing, China. The samples were fully dissolved in  $\text{HNO}_3$ , dried on a heating plate, and then redissolved using HCl and  $\text{H}_2\text{O}_2$ . Copper was eluted and extracted using anion exchange resin. More details are shown in [51,52]. The Cu isotope data were reported relative to the NIST976 standard, with a precision of  $\pm 0.1\%$  ( $2\sigma$ ) for  $\delta^{65}\text{Cu}$ .

## 4. Results

### 4.1. Hydrogen and Oxygen Isotopes

The H–O isotope results are listed in Table 1. The isotope fractionation equation utilized is  $\delta^{18}\text{O}_{\text{fluid}} = \delta^{18}\text{O}_{\text{quartz}} - (4.8 \times 1,000,000/T^2 - 4.77 \times 1000/T + 1.71)$  for quartz and fluid [53]. Here, T represents the absolute temperature at which quartz was formed. The  $\delta^{18}\text{O}$  values of the fluid were calculated using the homogeneous temperature of fluid inclusions from previous studies [24,34,54]. For the Chaoshan deposit, the  $\delta^{18}\text{O}_{\text{fluid}}$  values range from 3.2 to 5.9‰. In the Dongguashan deposit, the range is from 0.75 to 8.48‰, while in the Hucun deposit, the range extends from 5.7 to 10.3‰. As for the  $\delta\text{D}_{\text{fluid}}$  values of the same samples, they vary from  $-72.6$  to  $-63.4\%$ ,  $-70.1$  to  $58.5\%$ , and  $-88.1$  to  $-64.4\%$ , respectively.

**Table 1.** Hydrogen and oxygen isotopic compositions of the Chaoshan, Dongguashan, and Hucun deposits.

Deposit	Sample	Mineral	Occurrence	$\delta\text{D}_{\text{fluid}}$ (‰)	$\delta^{18}\text{O}_{\text{quartz}}$ (‰)	$\delta^{18}\text{O}_{\text{fluid}}$ (‰)	Th (°C)
Chaoshan Au deposit	CS-1	Quartz	Quartz–sulfide vein	−68.3	12.5	5.50	330 [54]
	CS-2	Quartz		−72.6	10.8	3.80	
	CS-5	Quartz		−63.4	10.2	3.20	
	CS-6	Quartz		−65.7	12.9	5.90	
Dongguashan Cu–(Au) deposit	DGS-1	Quartz	Quartz–sulfide vein in the stratiform orebody	−58.5	11.4	1.75	260 [24]
	DGS-2	Quartz		−65.4	10.4	0.75	
	DGS-3	Quartz		−59.5	12.9	3.25	
	DGS-10	Quartz	Quartz–sulfide vein in the porphyry orebody	−70.1	14.9	8.48	350 [24]
	DGS-11	Quartz		−66.9	12.3	5.88	
	DGS-12	Quartz		−62.1	13.5	7.08	
Hucun Cu–(Au) deposit	HC-1	Quartz	Quartz–sulfide vein	−88.1	14.1	6.10	300 [34]
	HC-2	Quartz		−64.4	13.7	5.70	
	HC-3	Quartz		−69.5	15.4	7.40	
	HC-8	Quartz	Quartz–molybdenite vein	−70.1	14.6	9.17	390 [34]
	HC-9	Quartz		−82.6	15.7	10.27	
	HC-10	Quartz		−83.3	12.5	7.07	

### 4.2. Carbon and Oxygen Isotopes

The C and O isotopic compositions of the calcite samples are provided in Table 2. The conversion equation used to calculate  $\delta^{18}\text{O}_{\text{SMOW}}$  is  $1.03086 \times \delta^{18}\text{O}_{\text{PDB}} + 30.86$  [55]. The C–O isotope ratios exhibit relatively uniform values. In the Chaoshan deposit, the values of  $\delta^{13}\text{C}_{\text{PDB}}$  range from  $-5.32$  to  $-4.33\%$ , and the values of  $\delta^{18}\text{O}_{\text{SMOW}}$  range from 12.45 to 14.62‰. In the Dongguashan deposit, the values of  $\delta^{13}\text{C}_{\text{PDB}}$  range from  $-7.13$  to  $-3.84\%$ , and the values of  $\delta^{18}\text{O}_{\text{SMOW}}$  range from 11.94 to 13.57‰. In the Hucun deposit, the values of  $\delta^{13}\text{C}_{\text{PDB}}$  range from  $-3.82$  to  $-2.26\%$ , and the values of  $\delta^{18}\text{O}_{\text{SMOW}}$  range from 11.86 to 12.76‰.

**Table 2.** Carbon and oxygen isotopic compositions of the Chaoshan, Dongguashan, and Hucun deposits.

Deposit	Sample	Mineral	Occurrence	$\delta^{13}\text{C}_{\text{PDB}}$ (‰)	$\delta^{18}\text{O}_{\text{PDB}}$ (‰)	$\delta^{18}\text{O}_{\text{SMOW}}$ (‰)
Chaoshan Au deposit	CS-9	Calcite	Calcite–quartz– pyrite vein	−4.33	12.5	12.46
	CS-10	Calcite		−5.32	10.8	13.11
	CS-11	Calcite		−5.01	10.2	14.62
Dongguashan Cu–(Au) deposit	DGS-4	Calcite	Calcite–quartz– pyrite vein	−6.86	11.4	12.74
	DGS-5	Calcite		−3.84	10.4	13.57
	DGS-9	Calcite		−7.13	12.9	11.94
	DGS-18	Calcite	Calcite–quartz– sulfide vein	−4.58	14.9	12.01
	DGS-19	Calcite		−6.94	12.3	13.00
	DGS-20	Calcite		−5.04	13.5	12.87
Hucun Cu–(Au) deposit	HC-16	Calcite	Calcite–pyrite vein	−2.26	14.1	11.94
	HC-22	Calcite		−2.42	13.7	12.77
	HC-25	Calcite		−3.82	15.4	11.86

#### 4.3. Sulfur Isotopes

The sulfur isotopic compositions of the sulfides are listed in Table 3. In the Chaoshan deposit, the  $\delta^{34}\text{S}$  values of pyrrhotite range from 4.56 to 7.63‰, with an average of 6.44‰. In the Dongguashan deposit, the  $\delta^{34}\text{S}$  values of the chalcopyrite range from 4.19 to 7.87‰, with an average of 5.83‰. In the Hucun deposit, the chalcopyrite samples exhibit  $\delta^{34}\text{S}$  values ranging from 1.95 to 3.28‰, with an average of 2.49‰, while the molybdenite samples have  $\delta^{34}\text{S}$  values between 4.74‰ and 5.25‰, with an average of 5.07‰.

**Table 3.** Sulfur, lead, and copper isotopic compositions of the Chaoshan, Dongguashan, and Hucun deposits.

Deposit	Sample	Mineral	Occurrence	$\delta^{34}\text{S}$ (‰)	$^{206}\text{Pb}/$ $^{204}\text{Pb}$	$^{207}\text{Pb}/$ $^{204}\text{Pb}$	$^{208}\text{Pb}/$ $^{204}\text{Pb}$	$\delta^{65}\text{Cu}$ (‰)
Chaoshan Au deposit	CS-13	Pyrrhotite	Pyrrhotite massive ore	6.58	18.388	15.502	38.456	0.17
	CS-14	Pyrrhotite		7.63	18.523	15.552	38.236	0.05
	CS-15	Pyrrhotite		4.56	18.563	15.645	38.263	−0.03
	CS-17	Pyrrhotite		6.98	18.272	15.535	38.321	0.12
Dongguashan Cu–(Au) deposit	DGS-6	Chalcopyrite	Cu-bearing serpentinite in the stratiform orebody	5.47	18.356	15.541	38.412	0.21
	DGS-7	Chalcopyrite		4.19	18.201	15.644	38.235	0.35
	DGS-8	Chalcopyrite		6.7	18.329	15.568	38.288	0.28
	DGS-14	Chalcopyrite	Disseminated chalcopyrite in the intrusion	5.31	18.252	15.623	38.313	−0.06
	DGS-15	Chalcopyrite		7.87	18.477	15.646	38.174	−0.13
	DGS-16	Chalcopyrite		5.45	18.52	15.582	38.352	−0.19
Hucun Cu–(Au) deposit	HC-12	Chalcopyrite	Chalcopyrite– molybdenite vein	3.28	18.168	15.525	38.185	−0.25
	HC-13	Chalcopyrite		1.95	18.216	15.573	38.354	−0.15
	HC-14	Chalcopyrite		2.23	18.281	15.554	38.164	−0.09
	HC-12	Molybdenite		5.23	No test			
	HC-13	Molybdenite		4.74				
	HC-14	Molybdenite		5.25				

#### 4.4. Lead Isotopes

Table 3 also presents the Pb isotopic compositions of sulfides, which exhibit a general consistency. In the Chaoshan deposit, the pyrrhotite samples display  $^{208}\text{Pb}/^{204}\text{Pb}$  ratios ranging from 38.236 to 38.456,  $^{207}\text{Pb}/^{204}\text{Pb}$  ratios ranging from 15.502 to 15.645, and  $^{206}\text{Pb}/^{204}\text{Pb}$  ratios ranging from 18.272 to 18.563. In the Dongguashan deposit, the chalcopyrite samples demonstrate  $^{208}\text{Pb}/^{204}\text{Pb}$  ratios ranging from 38.174 to 38.412,  $^{207}\text{Pb}/^{204}\text{Pb}$  ratios ranging from 15.541 to 16.646, and  $^{206}\text{Pb}/^{204}\text{Pb}$  ratios ranging from 18.201 to 18.52.

In the Hucun deposit, the chalcopyrite samples exhibit  $^{208}\text{Pb}/^{204}\text{Pb}$  ratios ranging from 38.164 to 38.354,  $^{207}\text{Pb}/^{204}\text{Pb}$  ratios ranging from 15.525 to 15.573, and  $^{206}\text{Pb}/^{204}\text{Pb}$  ratios ranging from 18.168 to 18.281.

#### 4.5. Copper Isotopes

The Cu isotopic compositions of pyrrhotite and chalcopyrite were analyzed to elucidate the origin of the copper element in mineralization (Table 3). In the Chaoshan deposit, the pyrrhotite samples demonstrate  $\delta^{65}\text{Cu}$  values ranging from  $-0.03$  to  $0.17$ ‰, with an average of  $0.08$ ‰. In the Dongguashan stratiform orebody, the chalcopyrite samples display  $\delta^{65}\text{Cu}$  values ranging from  $0.21$  to  $0.35$ ‰, with an average of  $0.28$ ‰, while in the Dongguashan porphyry orebody, the chalcopyrite samples exhibit  $\delta^{65}\text{Cu}$  values ranging from  $-0.19$  to  $-0.06$ ‰, with an average of  $-0.13$ ‰. The chalcopyrite samples in the Hucun deposit have  $\delta^{65}\text{Cu}$  values ranging from  $-0.25$  to  $-0.09$ ‰, with an average of  $-0.16$ ‰.

### 5. Discussion

#### 5.1. Origin of the Ore-Forming Fluids

The H–O isotopes of fluids provide valuable information for tracing the source and evolution of ore-forming fluids due to variations in hydrogen and oxygen isotopic compositions in water from different origins [56]. The  $\delta\text{D}_{\text{fluid}}$  and  $\delta^{18}\text{O}_{\text{fluid}}$  values obtained from quartz samples in the Chaoshan deposit, Dongguashan deposit, and Hucun deposit exhibit a consistent trend (Table 2). When plotted on the  $\delta\text{D}_{\text{fluid}}$  vs.  $\delta^{18}\text{O}_{\text{fluid}}$  diagram (Figure 5), the data points cluster near the primary magmatic water field, indicating that the ore-forming fluids were predominantly derived from magma [57,58]. Previous studies have reported that the oxygen isotope values of the regional mineralization-linked intrusions range from  $9.9$  to  $13.2$ ‰ [59,60]. The lower  $\delta^{18}\text{O}$  values in the ore-forming fluids suggest the presence of a certain amount of meteoric water mixed during the mineralization process.

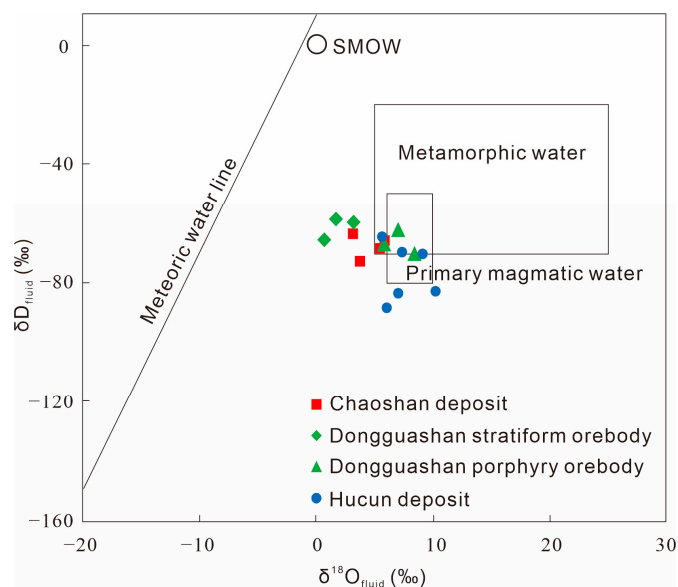


**Figure 5.**  $\delta\text{D}_{\text{fluid}}$  vs.  $\delta^{18}\text{O}_{\text{fluid}}$  diagram of the ore-forming fluids in the Chaoshan, Dongguashan, and Hucun deposits (Base diagram from [58]; meteoric water line from [57]).

Based on previous studies, three main sources of carbon are proposed in a hydrothermal metallogenic system [61–63]. These sources are the mantle or magma, characterized by  $\delta^{13}\text{C}$  values around  $-5$ ‰ [64]; marine carbonate, with  $\delta^{13}\text{C}$  values predominantly near  $0$ ‰ and ranging between  $-4$ ‰ and  $10$ ‰ [65]; and sedimentary organic matter, exhibiting  $\delta^{13}\text{C}$  values ranging from  $-30$  to  $-15$ ‰ [66]. The  $\delta^{13}\text{C}$  values of the three deposits are concentrated in the transitional area between the intrusion and marine carbonate, closer to the intrusion range (Figure 6), suggesting a possible origin of the hydrothermal fluids

from magma. Additionally, the  $\delta^{13}\text{C}$  values of the carbonate sediments in the Shizishan orefield [67,68] are significantly higher compared to the  $\delta^{13}\text{C}$  values of the three deposits, indicating an inconsistency between the ore-forming fluids and the stratigraphic materials.

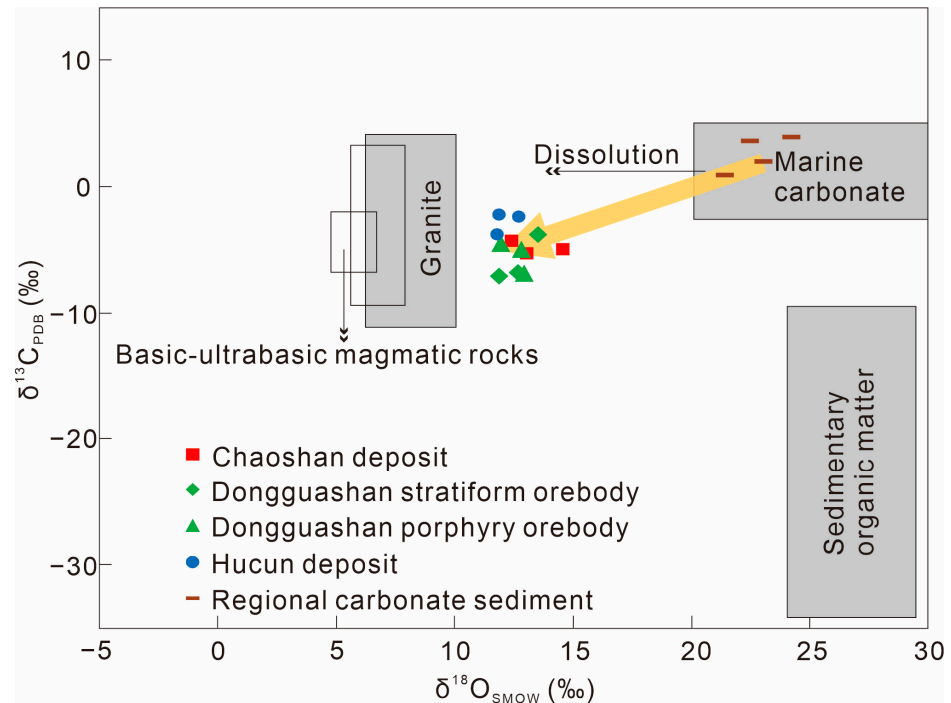


**Figure 6.**  $\delta^{13}\text{C}_{\text{PDB}}$  vs.  $\delta^{18}\text{O}_{\text{SMOW}}$  diagram of calcite in the Chaoshan, Dongguashan, and Hucun deposits (base diagram from [56,69]; regional carbonate sediment data from [67,68]).

## 5.2. Sulfur Source

The sulfur isotope ratios of sulfides are influenced by various factors, including the sulfur concentration, oxygen fugacity, pH, and temperature of the ore-forming fluids [70,71]. Past findings have demonstrated that when sulfates are either absent or occur in small amounts, sulfur in the ore-forming fluids predominantly exists in reduced substances such as  $\text{HS}^-$  and  $\text{S}^{2-}$ . In such cases, the sulfur isotopic composition of the ore-forming fluids can be represented by the sulfur isotopic composition of sulfides [70–72]. The absence of sulfates, such as barite or gypsum, during the mineralization stage in the Shizishan orefield points to sulfides as the dominant minerals and indicates that sulfur predominantly exists in its reduced form within the fluids. The obtained sulfur isotopic values of sulfides are relatively concentrated, exhibiting a tower-shaped distribution (Figure 7A). Therefore, the  $\delta^{34}\text{S}$  values of sulfides can be considered as approximations of the sulfur isotopic composition of the ore-forming fluids.

The  $\delta^{34}\text{S}$  values of the three ore deposits largely fall within the typical range of magmatic melt [66]. The  $\delta^{34}\text{S}$  values of the Mesozoic intrusions in the Tongling region range from 0.27‰ to 6.28‰ [73], suggesting that the sulfur in the ores shares a common magmatic source with intrusions. In the Chaoshan and Dongguashan deposits, a few individual sulfides exhibit  $\delta^{34}\text{S}$  values higher than 7‰, indicating a potential mixture of magmatic sulfur and sedimental sulfur. In the Tongling region, where gypsum layers are present in the Lower Carboniferous and Triassic strata, the  $\delta^{34}\text{S}$  values of gypsum and anhydrite typically range from 20‰ to 30‰ [30]. The incorporation of this high  $^{34}\text{S}$  component into the magmatic–hydrothermal fluids may result in higher  $\delta^{34}\text{S}$  values in the precipitated sulfides.

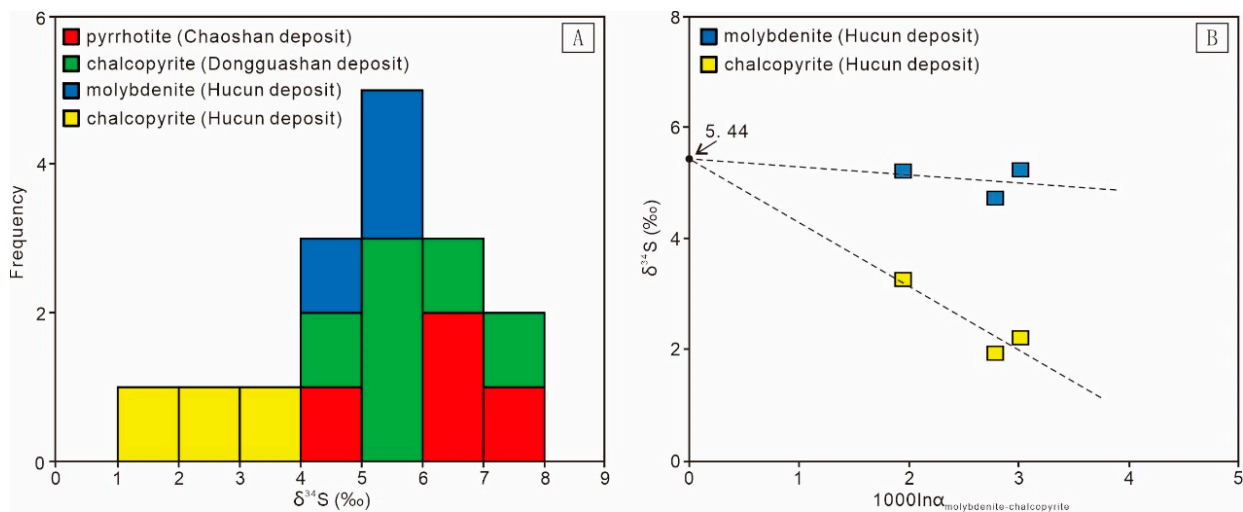


**Figure 7.** (A) Histogram of  $\delta^{34}\text{S}$  values for sulfides in the Chaoshan, Dongguashan, and Hucun deposits. (B) Plots of  $\delta^{34}\text{S}$  vs.  $1000\ln\alpha_{\text{molybdenite-chalcopyrite}}$  from Hucun deposit.

For the Hucun deposit, the  $\delta^{34}\text{S}$  values of molybdenite are higher than those of chalcopyrite, aligning with the enrichment sequence of  $^{34}\text{S}$  during sulfide crystallization [66]. This consistency indicates that the sulfur isotopic fractionation in the ore-forming fluids has reached an equilibrium state [71]. Assuming that mineral pairs (A and B) co-precipitate from a homogeneous system while experiencing varying temperature, the relationship between  $1000\ln\alpha_{\text{A-B}}$  and  $\delta^{34}\text{S}_{\text{A}}$  (or  $\delta^{34}\text{S}_{\text{B}}$ ) should exhibit a linear correlation, with the intercept of this line approximately equal to the  $\delta^{34}\text{S}$  value of the ore-forming system [74]. Specifically,  $1000\ln\alpha_{\text{A-B}} \approx \delta^{34}\text{S}_{\text{A}} - \delta^{34}\text{S}_{\text{B}}$ . By applying this method to calculate the sulfur isotopic values of molybdenite and chalcopyrite pairs from the Hucun deposit, a  $\delta^{34}\text{S}_{\text{fluid}}$  value of 5.44 is obtained (Figure 7B), indicating that the sulfur originates from a deep magmatic source.

### 5.3. Origin of Metals

The Pb isotopic compositions of the sulfides in the Shizishan ore field were plotted on the diagram of  $^{206}\text{Pb}/^{204}\text{Pb}$  vs.  $^{207}\text{Pb}/^{204}\text{Pb}$  (Figure 8A) and  $^{206}\text{Pb}/^{204}\text{Pb}$  vs.  $^{208}\text{Pb}/^{204}\text{Pb}$  (Figure 8B). The analysis reveals little variation in Pb isotopes among different deposits. Furthermore, the chalcopyrite samples obtained from both the stratiform orebody and the porphyry orebody in the Dongguashan deposit exhibit nearly identical Pb isotopes, suggesting a similar lead source. The majority of data points fall within the range of the mantle and upper crust, indicating a mixed crustal and mantle origin for Pb in the ores. Compared with the Pb isotopes of igneous and sedimentary rocks in the Tongling region [75], the sulfides have Pb isotopes that are generally consistent with the regional igneous rocks. Therefore, it can be inferred that the lead in the sulfides mainly derives from magmatic–hydrothermal fluids, although a minor contribution from sedimentary lead cannot be completely excluded.

The Cu isotopic compositions of the three ore deposits show little variation and are close to the average  $\delta^{65}\text{Cu}$  value of approximately 0 for the bulk earth silicate [76], implying a consistent copper source within the region. Unlike traditional C–H–O–S isotopes that provide indirect clues about the source and evolution of ore-forming materials, the Cu isotope offers direct indications of copper mineralization. Typically, the Cu isotopic ratios associated with magmatic processes exhibit limited variations, centered around zero, while low-temperature hydrothermal and sedimentary deposits tend to enrich in  $^{63}\text{Cu}$  [77]. However, for the porphyry–skarn mineralization system, the range of copper isotopic variations is broader, possibly due to the sequential precipitation of different Cu-bearing minerals [78] and the incorporation of wall-rock materials into the ore-forming fluids [79]. Previous experiments have demonstrated that the crystallization of minerals can

lead to copper isotopic fractionation, with preferential precipitation of  $^{63}\text{Cu}$  and gradual enrichment of  $^{65}\text{Cu}$  in the residual hydrothermal fluids. The  $\delta^{65}\text{Cu}$  value of the wall-rock marble in the Dongguashan deposit is 0.7‰ [76], significantly higher than the  $\delta^{65}\text{Cu}$  values of the chalcopyrite samples in the stratiform orebody, indicating that wall-rock components have a minor influence on the chalcopyrite precipitation. The lower  $\delta^{65}\text{Cu}$  values of chalcopyrite samples in the porphyry orebody compared to the stratiform orebody primarily arises from copper isotopic fractionation during the sulfide precipitation process, suggesting that the porphyry orebody formed prior to the stratiform orebody. By comparing it with the  $\delta^{65}\text{Cu}$  value of the Dongguashan quartz diorite [76], it is suggested that Cu in the Shizishan orefield mainly originates from magmatic–hydrothermal fluids (Figure 9).

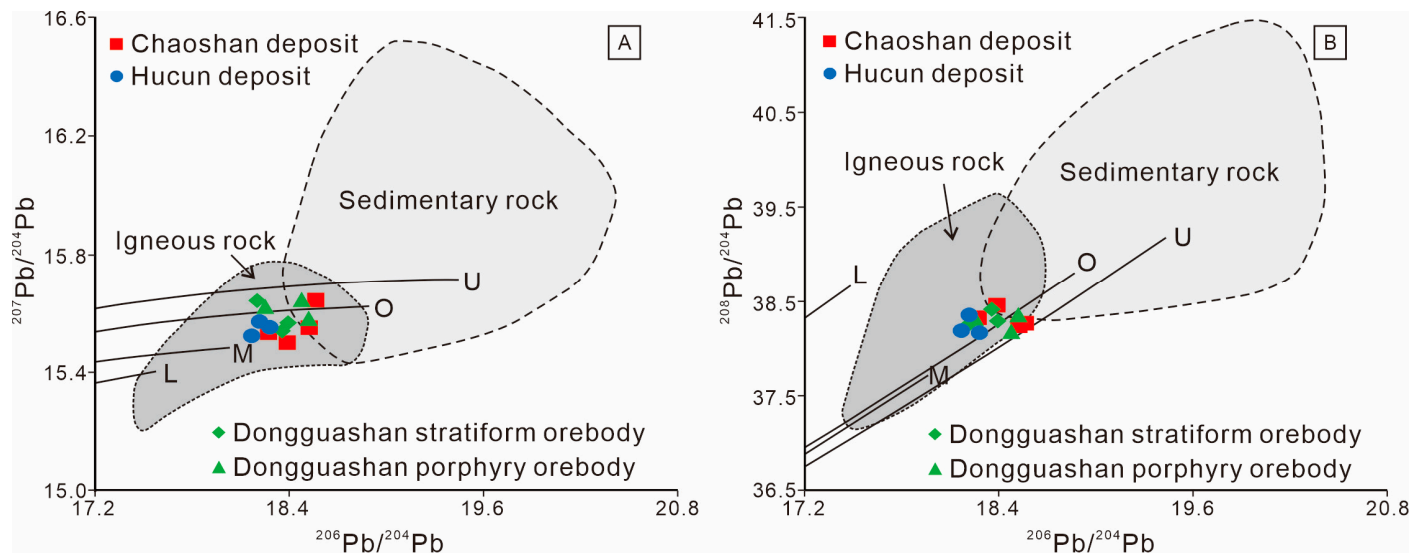


**Figure 8.** The diagrams show plots of  $^{206}\text{Pb}/^{204}\text{Pb}$  vs.  $^{207}\text{Pb}/^{204}\text{Pb}$  (A) and  $^{206}\text{Pb}/^{204}\text{Pb}$  vs.  $^{208}\text{Pb}/^{204}\text{Pb}$  (B) ratios of sulfides in the Chaoshan, Dongguashan, and Hucun deposits. The trends for the upper crust (U), orogenic belt (O), mantle (M), and lower crust (L) are taken from [80]. The fields for igneous rocks and sedimentary rocks are drawn using data from [75].

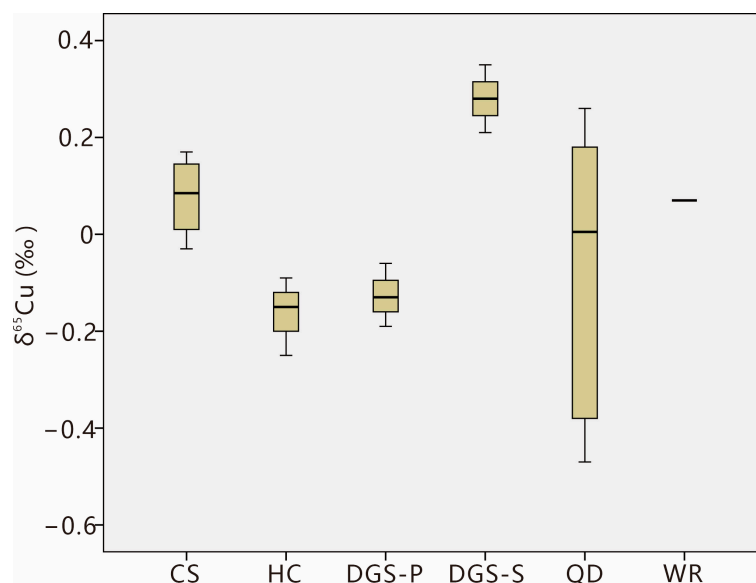


**Figure 9.** Histogram of  $\delta^{65}\text{Cu}$  values for sulfides in the Chaoshan, Dongguashan, and Hucun deposits. Abbreviations: CS = Chaoshan deposit; HC = Hucun deposit; DGS-P = Dongguashan porphyry orebody; DGS-S = Dongguashan stratiform orebody; QD = Dongguashan quartz diorite; WR = wall-rock marble in the Dongguashan deposit (QD and WR data from [76]).

#### 5.4. Genesis of the Shizishan Orefield

The origin of the stratiform orebodies in the unconformity interface between the Devonian and Carboniferous strata in the MLYMB has long been a subject of debate. The crux of the controversy lies in whether these orebodies were mainly formed by the Carboniferous sedimentary exhalative mineralization or by the Mesozoic magmatic–hydrothermal mineralization. However, based on our study of the Shizishan orefield, it seems that there may not be significant sedimentary exhalative mineralization in this area.

The geological cross-section map of the Dongguashan deposit indicates that the development of the stratiform orebodies was closely linked to the quartz diorite intrusion. The orebodies were mainly distributed around the intrusion, with thicker orebodies near the intrusion and thinner ones away from it until they pinched out (Figure 3C). This evidence contradicts the mechanism of sedimentary exhalative mineralization, which entails metallogenic fluids ascending along deep faults in a rift or oceanic spreading tectonic setting, resulting in the forming of orebodies through sedimentary exhalative activities. Such a process should have a regional extent and would not produce changes within a confined range from the intrusion to distant areas, causing orebodies to gradually vanish. If sedimentary exhalative activities occurred during the Carboniferous period, the contemporaneous sediments should show abnormalities of ore-forming elements near the exhalative vents, leaving discernible traces even in the region beyond the mining district far from the intrusion. However, the anomalies of ore-forming elements like Cu, Au, Ag, Pb, and Zn in the Tongling region are closely correlated with the distribution of the Mesozoic intrusions [43]. Additionally, the metallogenic alteration of the host rocks of the Dongguashan stratiform orebodies is primarily characterized by silicification, and the upper parts of the stratiform orebodies gradually transition into silicified orebodies, while the minerals of the stratiform orebodies are mainly derived from the retrograde alteration of magnesian skarn [81], which differs from the predominantly sedimentary exhalative mineralization. The formation mechanism of stratabound orebodies is believed to be influenced by lithological variations between Devonian siliceous rocks and Carboniferous calcareous rocks. These variations serve as structural weak planes that control the positioning of orebodies. They exert a significant pumping effect on magmatic–hydrothermal fluids, leading to the horizontal release of ore-forming substances along the unconformity surface [29]. This may explain why orebodies are confined to specific strata.

The main evidence for the sedimentary exhalative mineralization comes from field observations and isotope analysis of massive sulfides at the bottom unconformity interface of the Carboniferous strata. These factors encompass exhalative structures and the sedimentary origin of colloidal pyrite and strawberry pyrite, as well as sulfur isotope analysis of certain pyrite samples, which indicates their sedimentary source [21]. Undoubtedly, a substantial amount of sedimentary pyrite was developed near the bottom unconformity interface in the MLYMB. However, the pivotal question is whether the deposition of these pyrite particles was accompanied by the Cu–polymetallic mineralization. Hence, for the utilization of sulfur isotopic data derived from pyrite, it is imperative to rely on comprehensive microscopic observations and in situ microanalysis. Otherwise, the acquired data are prone to being a blend of values from diverse time periods, failing to accurately depict the actual ore-forming event. Therefore, the isotopic results of the sulfides related to Cu, Au, and Mo, namely chalcopyrite, pyrrhotite, and molybdenite, are evidently more reliable than the widely distributed pyrite in the region.

From multiple isotopic analysis, the stratiform-type and porphyry-type orebodies in the Dongguashan deposit, as well as in the Chaoshan deposit and the Hucun deposit, exhibit consistency in H–O–C–S–Pb–Cu isotopes. The findings suggest that porphyry–skarn–stratabound-type Cu–Au–Mo deposits of the Shizishan orefield belong to the same Mesozoic magmatic–hydrothermal metallogenic system. Furthermore, these results indicate a significant similarity in both the sources of ore-forming materials and the genesis of deposits between the stratabound copper sulfide deposits and the porphyry–skarn-type copper deposits in the MLYMB.

## 6. Conclusions

This paper examined three representative deposits in the Shizishan orefield: the Chaoshan skarn-type Au deposit, the Hucun porphyry–skarn-type Cu–Mo deposit, and the Dongguashan Cu–(Au) deposit, which has a disputed genesis of its stratiform orebodies. We investigated the ore genesis and sources of mineralized elements in the Shizishan orefield using H, O, C, S, Pb, and Cu isotopes. The main findings of our study are as follows:

- (1) The H–O isotopic compositions of hydrothermal quartz from the Chaoshan, Dongguashan, and Hucun deposits in the Shizishan orefield indicate that the hydrothermal fluids responsible for mineralization mainly originated from magmatic water mixed with some meteoric water. The C–O isotopic compositions of calcite show a large difference from the local sedimentary carbonates. The S isotopic compositions of sulfides reveal the characteristics of magmatic sulfur.
- (2) The Pb isotopic compositions in the three deposits are similar to those of the Shizishan intrusions, suggesting a predominantly magmatic source for lead. The Cu isotopic compositions of chalcopyrite and pyrrhotite demonstrate that Cu, the primary ore-forming element, was mainly derived from magmatic–hydrothermal fluids.
- (3) The Dongguashan stratiform orebodies, which are regarded as typical sedimentary exhalative mineralization in the previous controversy, are consistent in H–O–C–S–Pb–Cu isotopes with the Dongguashan porphyry orebodies and Chaoshan and Hucun deposits, implying a shared source of ore-forming materials and a common genetic origin.
- (4) From these findings, we conclude that the porphyry–skarn–stratabound-type Cu–Au–Mo deposits in the Shizishan orefield can be classified as a unified Mesozoic magmatic–hydrothermal metallogenic system. The stratabound copper sulfide deposits and the porphyry–skarn-type copper deposits share a notable resemblance in the source and genesis of ore-forming elements in the MLYMB.

**Author Contributions:** Conceptualization, J.L. and L.P.; methodology, J.L. and L.P.; software, Y.G.; validation, J.L. and Y.G.; formal analysis, J.L., Y.G. and S.L.; investigation, J.L. and S.L.; resources, L.P.; data curation, J.L. and Y.G.; writing—original draft preparation, J.L.; writing—review and editing, J.L., L.P. and Y.G.; visualization, Y.G. and S.L.; supervision, L.P.; project administration, J.L. and L.P.; funding acquisition, J.L. and L.P. All authors have read and agreed to the published version of the manuscript.

**Funding:** This research was funded by the Guizhou Provincial Science and Technology Project (QKHJC-ZK[2021] YB211) and the Science and Technology Project of Jiangxi Education Department (GJJ201346).

**Data Availability Statement:** Not applicable.

**Acknowledgments:** Thanks to Geological Team 321 of the Geology and Mineral Exploration Bureau of Anhui Province and Tongling Nonferrous Metals Group Holdings Co., Ltd. for providing technical and logistical support during field and sampling activities.

**Conflicts of Interest:** The authors declare that they have no known competing financial interest or personal relationships that could have appeared to influence the work reported in this paper.

## References

1. Chang, Y.F.; Liu, X.P.; Wu, Y.C. *The Copper-Iron Belt of the Middle and Lower Reaches of the Changjiang River*; Geological Publishing House: Beijing, China, 1991; pp. 1–379, (In Chinese with English Abstract).
2. Mao, J.W.; Xie, G.Q.; Duan, C.; Pirajno, F.; Lshiyama, D.; Chen, Y.C. A tectono-genetic model for porphyry-skarn-stratabound Cu-Au-Mo-Fe and magnetite-apatite deposits along the Middle-lower Yangtze River Valley, Eastern China. *Ore Geol. Rev.* **2011**, *43*, 294–314. [[CrossRef](#)]
3. Zhou, T.F.; Wang, S.W.; Fan, Y.; Yuan, F.; Zhang, D.Y.; White, N.C. A review of the intracontinental porphyry deposits in the Middle-lower Yangtze River Valley metallogenic belt, Eastern China. *Ore Geol. Rev.* **2015**, *65*, 433–456. [[CrossRef](#)]
4. Jiang, S.Y.; Ma, F.; Zhao, K.D.; Jiang, Y.H.; Ling, H.F.; Ni, P. Origin of iron deposits in the Ningwu volcanic basin, Lower Yangtze River district, China: Geochemical and isotopic evidence. *Geochim. Cosmochim. Acta* **2006**, *70*, A293. [[CrossRef](#)]

5. Li, J.W.; Chen, J.H.; Zeng, J.N.; Lu, J.P.; Zhang, Y.X.; Li, X.F.; Wu, Y.F.; Lu, S.F. SHRIMP zircon U–Pb dating of gabbro-diorite porphyrite in Jishan iron ore deposit of Ningwu basin and its geological significance. *Miner. Depos.* **2012**, *31*, 1227–1236, (In Chinese with English Abstract).
6. Yu, J.J.; Lu, B.C.; Wang, T.Z.; Che, L.R. Cretaceous Cu-Au, pyrite, and Fe-oxide-apatite deposits in the Ningwu basin, Lower Yangtze Area, Eastern China. *J. Asian Earth Sci.* **2015**, *103*, 150–168. [[CrossRef](#)]
7. Xu, K.Q.; Zhu, J.C. Origin of the sedimentary- (or volcano sedimentary-) iron-copper deposits in some faults depression belts in southeast China. *Fujian Geol.* **1978**, *4*, 1–68, (In Chinese with English Abstract).
8. Gu, L.X.; Xu, K.Q. On the Carboniferous submarine massive sulfide deposits in the Lower Reaches of the Changjiang (Yangzi) River. *Acta Geol. Sin.* **1986**, *2*, 176–188, (In Chinese with English Abstract).
9. Xu, G.; Zhou, J. The Xinqiao Cu-S-Fe-Au deposit in the Tongling mineral district, China: Synorogenic remobilization of a stratiform sulfide deposit. *Ore Geol. Rev.* **2001**, *18*, 77–94. [[CrossRef](#)]
10. Guo, W.; Lu, J.; Jiang, S.; Zhang, R.; Qi, L. Re-Os isotope dating of pyrite from the footwall mineralization zone of the Xinqiao deposit, Tongling, Anhui Province: Geochronological evidence for submarine exhalative sedimentation. *Chin. Sci. Bull.* **2011**, *56*, 3860–3865, (In Chinese with English Abstract). [[CrossRef](#)]
11. Wang, Y.Y.; Xiao, Y.L.; Yang, X.Y. Re-Os isotope systematics and fluid inclusions of Xinqiao deposit in Tongling, the Middle-Lower Yangtze River Metallogenic Belt. *Acta Petrol. Sin.* **2015**, *31*, 1031–1039, (In Chinese with English Abstract).
12. Zhai, Y.S.; Yao, S.Z.; Lin, X.D.; Jin, F.Q.; Zhou, X.R.; Wan, T.F.; Zhou, Z.G. *Metallogenic of Iron-Copper-(Gold) Deposits of the Middle and Lower Reaches of Changjiang River*; Geological Publishing House: Beijing, China, 1992; p. 235. (In Chinese)
13. Xu, X.C.; Yin, T.; Lou, J.W.; Lu, S.M.; Xie, Q.Q.; Chu, P.L. Origin of Dongguashan stratabound Cu-Au skarn deposit in Tongling: Restraints of sulfur isotope. *Acta Petrol. Sini.* **2010**, *26*, 2739–2750, (In Chinese with English Abstract).
14. Li, J.W. Research on Metallogenic Regularities of Cu-Au-Mo Deposits in the Shizishan Ore Field, Tongling, Anhui Province. Master's Thesis, University of Geosciences, Wuhan, China, 2013; pp. 42–68, (In Chinese with English Abstract).
15. Wang, Y.; Zhu, X.K.; Cheng, Y.B.; Li, Z.H. Ore microscopy & Fe isotope of the Xinqiao deposit and their constraints on the ore genesis. *J. Jilin Univ. (Earth Sci. Ed.)* **2013**, *43*, 1787–1798, (In Chinese with English Abstract).
16. Li, Y.; Li, J.-W.; Li, X.-H.; Selby, D.; Huang, G.-H.; Chen, L.-J.; Zheng, K. An early Cretaceous carbonate replacement origin for the Xinqiao stratabound massive sulfide deposit, Middle-Lower Yangtze metallogenic belt, China. *Ore Geol. Rev.* **2017**, *80*, 985–1003. [[CrossRef](#)]
17. Zhang, Y.; Shao, Y.J.; Chen, H.Y.; Liu, Z.F.; Li, D.F. A hydrothermal origin for the large Xinqiao Cu-S-Fe deposit, eastern China: Evidence from sulfide geochemistry and sulfur isotopes. *Ore Geol. Rev.* **2017**, *88*, 534–549. [[CrossRef](#)]
18. Xie, J.C.; Ge, L.K.; Fang, D.; Li, Q.Z.; Qian, L.; Li, Z.S.; Yan, J.; Sun, W.D. Geochemistry of pyrite from stratabound massive sulfide deposits, Tongling region, China: Implication for their genesis. *Ore Geol. Rev.* **2020**, *120*, 103430. [[CrossRef](#)]
19. Xiao, X.; Zhou, T.F.; White, N.C.; Fan, Y.; Zhang, L.J.; Chen, X.F. Porphyry Cu mineralization processes of Xinqiao deposit, Tongling ore district: Constraints from the geochronology and geochemistry of zircon, apatite, and rutile. *Ore Geol. Rev.* **2021**, *138*, 104340. [[CrossRef](#)]
20. Wang, Y.; Yang, X.Y.; Wang, C.T.; Zhang, H.S.; Liu, S.S.; Sun, C. Comparative studies on stratabound and skarn-type deposits, Tongling region, lower Yangtze River metallogenic Belt: Constraints from pyrite geochemistry. *Ore Geol. Rev.* **2022**, *146*, 104919. [[CrossRef](#)]
21. Yang, Z.S.; Hou, Z.Q.; Meng, Y.F.; Zeng, P.S.; Li, H.Y.; Xu, W.Y.; Tian, S.H.; Wang, X.C.; Yao, X.D.; Jiang, Z.P. Spatial-temporal structures of Hercynian exhalative-sedimentary fluid system in Tongling ore concentration area, Anhui Province. *Miner. Depos.* **2004**, *23*, 281–297, (In Chinese with English Abstract).
22. Xu, W.Y.; Yang, Z.S.; Meng, Y.F.; Zeng, P.S.; Shi, D.N.; Tian, S.H.; Li, H.Y. Genetic model and dynamic migration of ore-forming fluids in carboniferous exhalation-sedimentary massive sulfide deposits of Tongling district, Anhui Province. *Miner. Depos.* **2004**, *23*, 353–364, (In Chinese with English Abstract).
23. Li, H.Y.; Li, Y.J.; Hou, Z.Q.; Yang, Z.S.; Meng, Y.F.; Zeng, P.S.; Xu, W.Y. Geochemical features of the Xinqiao massive sulfide deposit in Anhui Province. *Chin. J. Geol.* **2005**, *40*, 337–345, (In Chinese with English Abstract).
24. Liu, Z.-F.; Shao, Y.-J.; Wang, C.; Liu, Q.-Q. Genesis of the Dongguashan skarn Cu-(Au) deposit in Tongling, Eastern China: Evidence from fluid inclusions and HOS-Pb isotopes. *Ore Geol. Rev.* **2019**, *104*, 462–476. [[CrossRef](#)]
25. Xie, H.G.; Wang, W.B.; Li, W.D. The genesis and metallogenic epoch of Xinqiao Cu-S deposit, Anhui. *Volcanol. Miner. Resour.* **1995**, *16*, 101–107, (In Chinese with English Abstract).
26. Wang, Y.B.; Tang, S.H.; Wang, J.H.; Zeng, P.S.; Yang, Z.S.; Meng, Y.F.; Tian, S.H. Rb-Sr dating the pyrite of the Xinqiao Cu-S-Fe-Au deposit, Tongling, Anhui Province. *Geol. Rev.* **2004**, *50*, 538–541, (In Chinese with English Abstract).
27. Xie, J.C.; Yang, X.Y.; Du, J.G.; Du, X.W.; Xiao, Y.L.; Qu, W.J.; Sun, W.D. Re-Os precise dating of pyrite from the Xinqiao Cu-Au-Fe-S deposit in Tongling, Anhui and its implications for mineralization. *Geol. Sci.* **2009**, *44*, 183–192, (In Chinese with English Abstract).
28. Zhang, Y.; Shao, Y.J.; Quan, W.; Liu, Z.F.; Liu, Q.Q. Rb-Sr isotope dating of the fluid inclusions in quartz form quartz-pyrite veins in the footwall of Xinqiao Cu-S-Fe deposit, Tongling. *Geol. Rev.* **2015**, *61*, 1168–1176, (in Chinese with English abstract).
29. Mao, J.W.; Stein, H.; Du, A.D.; Zhou, T.F.; Mei, Y.X.; Li, Y.F.; Zang, W.S.; Li, J.W. Molybdenite Re-Os precise dating for molybdenite from Cu-Au-Mo deposits in the middle-lower reaches of Yangtze river belt and its implications for mineralization. *Acta Geol. Sini.* **2004**, *78*, 121–131, (In Chinese with English Abstract).

30. Lu, S.M. The Magmatism and Fluid Mineralization in Shizishan Copper-Gold Ore-Field of Tongling, Anhui Province. Ph.D. Thesis, Hefei University of Technology, Hefei, China, 2007; p. 158, (In Chinese with English Abstract).
31. Qu, H.Y.; Pei, F.R.; Wang, Y.L.; Li, J.W. Re-Os dating of molybdenite from the Fenghuangshan skarn Cu deposit in Tongling, Anhui Province and its geological significance. *Acta Petrol. Sin.* **2010**, *26*, 785–796, (In Chinese with English Abstract).
32. Pan, L.C.; Hu, R.Z.; Qyebamiji, A.; Wu, H.Y.; Li, J.W.; Li, J.X. Contrasting magma compositions between Cu and Au mineralized granodiorite intrusions in the Tongling ore district in South China using apatite chemical composition and Sr-Nd isotopes. *Am. Mineral.* **2021**, *106*, 1873–1889. [[CrossRef](#)]
33. Xie, J.C.; Zhang, X.; Huang, S.; Ge, L.K.; Li, Q.Z.; Sun, W.D. Genesis of Chaoshan skarn Au deposit, Tongling, eastern China: Insights from mineral geochemistry. *J. Geochem. Explor.* **2022**, *241*, 107055. [[CrossRef](#)]
34. Cao, Y.; Zheng, Z.J.; Du, Y.L.; Gao, F.P.; Qin, X.L.; Yang, H.M.; Lu, Y.H.; Du, Y.S. Ore geology and fluid inclusions of the Hucunna deposit, Tongling, Eastern China: Implications for the separation of copper and molybdenum in skarn deposits. *Ore Geol. Rev.* **2017**, *81*, 925–939. [[CrossRef](#)]
35. Pan, L.C.; Hu, R.Z.; Liu, Q.; Li, J.W.; Li, J.X. Titanite geochemistry and its indicators for Cu-mineralized magmas: Insight from three dioritic intrusions in the Tongling area of the Lower Yangtze River metallogenic belt. *Ore Geol. Rev.* **2022**, *151*, 105219. [[CrossRef](#)]
36. Chen, K.; Shao, Y.J.; Zhang, J.K.; Zhang, Y.; Tan, H.J.; Zhang, Y.C.; Liu, Z.F. Garnet U-Pb geochronology and geochemistry reveal deposit types and fluid evolution: An example from the Dongguashan Cu-Au deposit, eastern China. *Ore Geol. Rev.* **2022**, *145*, 104883. [[CrossRef](#)]
37. Xu, J.F.; Shinjo, R.; Defant, M.J.; Wang, Q.; Rapp, R.P. Origin of Mesozoic adakitic intrusive rocks in the Ningzhen area of east China: Partial melting of delaminated lower continental crust. *Geology* **2002**, *30*, 1111–1114. [[CrossRef](#)]
38. Wang, Q.; Wyman, D.A.; Xu, J.F.; Zhao, Z.H.; Jian, P.; Xiong, X.L.; Bao, Z.W.; Li, C.F.; Bai, Z.H. Petrogenesis of Cretaceous adakitic and shoshonitic igneous rocks in the Luzong area, Anhui Province (eastern China): Implications for geodynamics and Cu-Au mineralization. *Lithos* **2006**, *89*, 424–446. [[CrossRef](#)]
39. Zhou, X.M.; Sun, T.; Shen, W.Z.; Shu, L.S.; Niu, Y.L. Petrogenesis of Mesozoic granitoids and volcanic rocks in South China: A response to tectonic evolution. *Episodes* **2006**, *29*, 26–33. [[CrossRef](#)]
40. Sun, W.D.; Ding, X.; Hu, Y.H.; Li, X.H. The golden transformation of the Cretaceous plate subduction in the west Pacific. *Earth Planet. Sc. Lett.* **2007**, *262*, 533–542. [[CrossRef](#)]
41. Wang, J.Z.; Li, J.W.; Zhao, X.F.; Qian, Z.Z.; Ma, C.Q. Genesis of the Chaoshan gold deposit and its host intrusion, Tongling area: Constraints from  $^{40}\text{Ar}/^{39}\text{Ar}$  ages and elemental and Sr-Nd-O-C-S isotope geochemistry. *Acta Petrol. Sin.* **2008**, *24*, 1875–1888, (In Chinese with English Abstract).
42. Einaudi, M.T.; Burt, D.M. Introduction, terminology, classification, and composition of skarn deposits. *Econ. Geol.* **1982**, *77*, 745–754. [[CrossRef](#)]
43. Lu, S.F.; Zeng, J.N.; Li, J.W.; Wu, Y.F.; Li, X.F. Geochronology and geochemistry of the Hucunna granodiorite in the Shizishan area, Tongling. *Bull. Mineral. Petrol. Geochem.* **2014**, *33*, 355–365.
44. Yang, H.M.; Du, Y.S.; Lu, Y.H.; Chen, L.J.; Zheng, Z.J.; Zhang, Y. U-Pb and Re-Os geochronology of the Hucunna copper-molybdenum deposit in Anhui Province, Southeast China, and its geological implications. *Resour. Geol.* **2016**, *66*, 303–312. [[CrossRef](#)]
45. Guo, W.; Lu, J.; Zhang, R.; Xu, Z. Ore textures and genetic significance of pyrrhotite from Dongguashan ore deposit in Tongling area, Anhui Province. *Miner. Depos.* **2010**, *29*, 405–414, (In Chinese with English Abstract).
46. Clayton, R.N.; Mayeda, T.K. The use of bromine pentafluoride in the extraction of oxygen from oxides and silicates for isotopic analysis. *Geochim. Cosmochim. Acta* **1963**, *27*, 43–52. [[CrossRef](#)]
47. Friedman, I. Deuterium content of natural water and other substances. *Geochim. Cosmochim. Acta* **1953**, *4*, 89–103. [[CrossRef](#)]
48. McCrea, J.M. On the isotopic chemistry of carbonates and a paleotemperature scale. *J. Chem. Phys.* **1950**, *18*, 849–857. [[CrossRef](#)]
49. Robinson, B.W.; Kusakabe, M. Quantitative preparation of sulfur dioxide, for  $^{34}\text{S}/^{32}\text{S}$  analyses, from sulfides by combustion with cuprous oxide. *Anal. Chem.* **1975**, *47*, 1179–1181. [[CrossRef](#)]
50. Li, S.N.; Ni, P.; Bao, T.; Wang, G.-G.; Chi, Z.; Li, W.-S.; Zhu, R.-Z.; Dai, B.-Z.; Xiang, H.-L. Geological, fluid inclusion, and H-O-S-Pb isotopic studies of the Xiaban epithermal gold deposit, Fujian Province, southeast China: Implications for ore genesis and mineral exploration. *Ore Geol. Rev.* **2020**, *117*, 103280. [[CrossRef](#)]
51. Maréchal, C.N.; Telouk, P.; Albarede, F. Precise analysis of copper and zinc isotopic compositions by plasma source mass spectrometry. *Chem. Geol.* **1999**, *156*, 251–273. [[CrossRef](#)]
52. Mathur, R.; Ruiz, J.; Titley, S.; Liermann, L.; Buss, H.; Brantley, S. Cu isotopic fractionation in the supergene environment with and without bacteria. *Geochim. Cosmochim. Acta* **2005**, *69*, 5233–5246. [[CrossRef](#)]
53. Matsuhisa, Y.; Goldsmith, J.; Clayton, R. Oxygen isotopic fractionation in the system quartz-albite-anorthite-water. *Geochim. Cosmochim. Acta* **1979**, *43*, 1131–1140. [[CrossRef](#)]
54. Yang, X.N.; Xu, Z.W.; Gao, G.; Lu, X.C.; Liu, S.M.; Li, H.Y. Fluid inclusion studies of the Chaoshan gold deposit in Tongling, Anhui Province, China. *Acta Petrol. Sin.* **2008**, *24*, 1889–1899, (In Chinese with English Abstract).
55. Friedman, I.; O'Neil, J.R. Compilation of stable isotope fractionation factors of geochemical interest. *Data Geochem.* **1977**, *440*-KK, 1–12.

56. Taylor, H.P. Oxygen and hydrogen isotope relationships in hydrothermal mineral deposits. In *Geochemistry of Hydrothermal Ore Deposits*, 2nd ed.; Barnes, H.L., Ed.; Wiley: New York, NY, USA, 1979; pp. 236–277.
57. Epstein, S.; Sharp, R.P.; Gow, A.J. Six-year record of oxygen and hydrogen isotope variations in South Pole firn. *J. Geophys. Res.* **1965**, *70*, 1809–1814. [[CrossRef](#)]
58. Sheppard, S.M.F. Characterization and isotopic variations in natural waters. *Rev. Mineral. Geochem.* **1986**, *16*, 165–183.
59. Xu, Z.W.; Lu, X.C.; Gao, G.; Fang, C.Q.; Wang, Y.J.; Yang, X.N.; Jiang, S.Y.; Chen, B.G. Isotope geochemistry and mineralization in the Dongguashan diplogenic stratified copper deposit, Tongling area. *Geol. Rev.* **2007**, *53*, 44–51, (In Chinese with English Abstract).
60. Xu, X.C.; Bai, R.Y.; Xie, Q.Q.; Lou, J.W.; Zhang, Z.Z.; Liu, Q.N.; Chen, L.W. Re-understanding of the geological and geochemical characteristics of the Mesozoic intrusive rocks from Tongling area of Anhui Province, and discussions on their genesis. *Acta Petrol. Sini.* **2012**, *28*, 3139–3169, (In Chinese with English Abstract).
61. Taylor, H.P.; Frechen, J.; Degens, E.T. Oxygen and carbon isotope studies of carbonatites from the Laacher See District, West Germany and the Alno District, Sweden. *Geochim. Cosmochim. Acta* **1967**, *31*, 407–430. [[CrossRef](#)]
62. Veizer, J.; Hoefs, J. The nature of O18/O16 and C13/C12 secular trends in sedimentary carbonate rocks. *Geochim. Cosmochim. Acta* **1976**, *40*, 1387–1395. [[CrossRef](#)]
63. Demény, A.; Ahijado, A.; Casillas, R.; Vennemann, T.W. Crustal contamination and fluid/rock interaction in the carbonatites of Fuerteventura (Canary Islands, Spain): A C, O, H isotope study. *Lithos* **1998**, *44*, 101–115. [[CrossRef](#)]
64. Ohmoto, H. Stable isotope geochemistry of ore deposits. *Rev. Mineral. Geochem.* **1986**, *16*, 491–559.
65. Schidlowski, M.; Aharon, P. Carbon cycle and carbon isotope record: Geochemical impact of life over 3.8 Ga of Earth history. In *Early Organic Evolution*; Springer: Berlin/Heidelberg, Germany, 1992; pp. 147–175.
66. Hoefs, J. *Stable Isotope Geochemistry*, 6th ed.; Springer: Berlin/Heidelberg, Germany, 2009; pp. 1–285.
67. Tian, S.H.; Ding, T.P.; Yang, Z.S. REE and stable isotope geochemical characteristics of Chaoshan gold deposit in Tongling, Anhui Province. *Miner. Depos.* **2004**, *23*, 365–374, (In Chinese with English Abstract).
68. Gao, G.; Xu, Z.W.; Yang, X.N. Petrogenesis of the Baimangshan pyroxene diorite intrusion in Tongling area, Anhui Province: Constraints from Sr-Nd-Pb-O isotopes. *J. Nanjing Univ. (Natural Sci.)* **2006**, *42*, 269–279, (In Chinese with English Abstract).
69. Deines, P. Stable isotope variations in carbonatites. In *Carbonatites: Genesis and Evolution*; Bell, K., Ed.; Unwin Hyman: London, UK, 1989; pp. 301–359.
70. Ohmoto, H. Systematics of sulfur and carbon isotopes in hydrothermal ore deposit. *Econ. Geol. Bull. Soc.* **1972**, *67*, 551–578. [[CrossRef](#)]
71. Ohmoto, H.; Goldhaber, M.B. Sulfur and carbon isotopes. In *Geochemistry of Hydrothermal Ore Deposits*, 3rd ed.; Barnes, H.L., Ed.; Wiley: New York, NY, USA, 1997; pp. 517–611.
72. Seal, R.R. Sulfur isotope geochemistry of sulfide minerals. *Rev. Mineral. Geochem.* **2006**, *61*, 633–677. [[CrossRef](#)]
73. Li, J.; Pei, R.; Zhang, D.; Mei, Y.; Zang, W.; Meng, G.; Zeng, P.; Li, T. Geochemical characteristics of the Yanshanian intermediate-acid intrusive rocks in the Tongling mineralization concentration area, Anhui Province, and their geological implications. *Acta Geosci. Sin.* **2007**, *1*, 11–22, (In Chinese with English Abstract).
74. Pinckney, D.M.; Rafter, T.A. Fractionation of sulfur isotopes during ore deposition in the upper Mississippi Valley Zinc-Lead district. *Econ. Geol.* **1972**, *67*, 315–327. [[CrossRef](#)]
75. Lou, J.W. Intermediate-Acid Intrusive Rocks of Tongling Ore District and Copper-Polymetallic Deposits of Shizishan Ore-Field, Anhui Province. Ph.D. Thesis, Hefei University of Technology, Hefei, China, 2012; pp. 1–223, (In Chinese with English Abstract).
76. Wang, Y.; Zhu, X.K.; Mao, J.W.; Cheng, Y.B.; Li, Z.H. Preliminary study on Cu isotopic geochemistry behavior of Dongguashan porphyry-skarn deposit, Tongling district. *Acta Geol. Sini.* **2014**, *88*, 2413–2422, (In Chinese with English Abstract).
77. Larson, P.B.; Maher, K.; Ramos, F.C.; Chang, Z.; Gaspar, M.; Meinert, L.D. Copper isotope ratios in magmatic and hydrothermal ore-forming environments. *Chem. Geol.* **2003**, *201*, 337–350. [[CrossRef](#)]
78. Graham, S.; Pearson, N.; Jackson, S. Tracing Fe and Cu from source to porphyry: In situ determination of Cu and Fe isotope ratios in sulfides from the Grasberg Cu-Au deposit. *Chem. Geol.* **2004**, *207*, 147–169. [[CrossRef](#)]
79. Mathur, R.; Ruiz, J.; Casselman, M.J. Use of Cu isotopes to distinguish primary and secondary Cu mineralization in the Canariaco Norte porphyry copper deposit, Northern Peru. *Miner. Depos.* **2012**, *47*, 755–762. [[CrossRef](#)]
80. Zartman, R.; Doe, B. Plumbotectonics: The model. *Tectonophysics* **1981**, *75*, 135–162. [[CrossRef](#)]
81. Mao, J. Mineral deposit model for porphyry-skarn polymetallic copper deposits in Tongling ore dense district of Middle-Lower Yangtze Valley metallogenic belt. *Miner. Depos.* **2009**, *28*, 109–119, (In Chinese with English abstract).

**Disclaimer/Publisher’s Note:** The statements, opinions and data contained in all publications are solely those of the individual author(s) and contributor(s) and not of MDPI and/or the editor(s). MDPI and/or the editor(s) disclaim responsibility for any injury to people or property resulting from any ideas, methods, instructions or products referred to in the content.